Accepted for publication in the 1998 IEEE ICRA Proceedings, Leuven, Belgium, May 16-21

Integrated Precision 3-DOF Position Sensor for Planar Linear Motors

Zack J. Butler, Alfred A. Rizzi, and Ralph L. Hollis
The Robotics Institute, Carnegie Mellon University
{zackb, arizzi, rhollis}@ri.cmu.edu

Abstract

Planar linear motors have been shown to be capable of fast accurate 2-DOF motions making them useful for assembly tasks. However, the lack of sensing capability has limited their applications. Previous planar motor sensors have been precise but bulky and sensed only a single direction of motion. We present a small integrated 3-DOF sensor capable of 0.2 μm position resolution (1σ) which has been integrated with an existing planar linear motor without changing its overall size. Physical design of the sensor is presented as well as the custom electronics used to attain a low-noise DC output from the small signal levels of the sensor. Finally, we present results that demonstrate the resolution and accuracy of the complete sensor system.

1 Introduction

As electromechanical products have decreased in size, manufacturing them has become more challenging. Specifically, applications such as circuit board assembly and testing and disk drive assembly require high throughput and micron-level precision. Planar linear motors are well-suited to these tasks since they provide both high velocity and fine motion capability in two dimensions with a single moving part. In addition, multiple motors can share a workspace, allowing for more efficient space utilization. They are commercially available and have been used in various industrial applications without position sensing with some success [1]. However, they have not been widely accepted because they tend to suffer from loss of synchrony at high speeds and are unable to reject disturbances. The addition of high-precision sensing would alleviate these drawbacks, increasing both speed and robustness, making these motors more attractive for automated assembly.

In the Microdynamic Systems Laboratory[1] at Carnegie Mellon University, we are developing hardware and software components of a small modular factory system, or *minifactory*. These include planar linear motors as the moving elements of *couriers*, autonomous robots that shuttle assemblies from one station to the next and cooperate with overhead robots to perform precision assembly tasks [2].

Planar linear motors are essentially stepper motors that consist of a forcer that moves over a planar steel platen surface. The forcer floats 12–15 μm above the platen on an air bearing, the air for which is provided along with electrical power in a single tether. The platen surface provides a grid of stator teeth and is backfilled with epoxy to provide a flat surface for the air bearing. The forcer has the potential for submicron motion resolution and velocities of 2 m/s, but these capabilities cannot be reliably exercised under open-loop control.

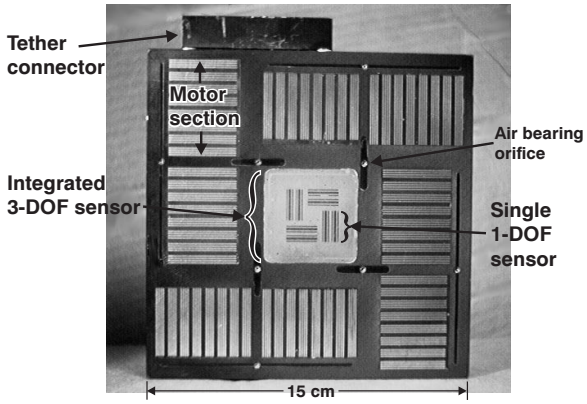

Figure 1: Commercial planar linear motor forcer with integrated 3-DOF platen sensor.

To support closed-loop control that exploits these abilities of the motor, a planar motor sensor should have micron-level resolution in translation and equivalent sensitivity to rotation, and be able to support variable sampling rates of at least 5 kHz. The sensor should also be compact, fitting within the footprint of the forcer, including all electronics, and should directly interface to the controlling computer.

Previous platen sensors have sensed (or proposed to sense) the platen teeth magnetically, optically [3], and capacitively [4]. Of the three sensing modalities, magnetic sensing has received the most attention since it takes advantage of the distinct characteristics of the steel teeth and epoxy fill and has the potential for easy integration with commercially available forcers and platens. Crawford and others at MIT developed a one-axis magnetic sensor capable of 4 μm resolution [5]. Ish-Shalom presents a sensor capable of sub-micron resolution in a single dimension [6]. The sensor we have developed has sub-micron resolution in two dimensions and also senses orientation while being smaller and easier to reliably fabricate than previous

[1] http://www.cs.cmu.edu/~msl

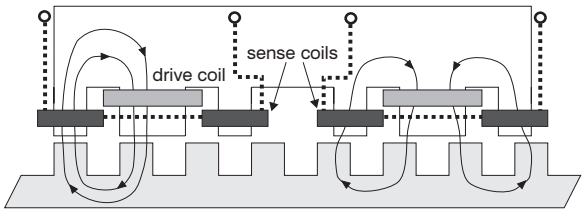

Figure 2: Cross-section view of a quadrature pair of platen sensors with approximate magnetic flux paths.

designs.

This sensor is based on preliminary work by Brennemann and Hollis, outlined in [7], in which a one-dimensional sensor was designed and fabricated. Although the general concept of the current sensor is not entirely novel, the modeling and surrounding circuitry is different than in previous designs, and the fabrication is quite different. These differences allow this sensor to achieve sub-micron resolution at a 14 kHz sampling rate, while being compact enough to fit inside the forcer, as can be seen in Fig. 1.

2 Magnetic platen sensor operation

Magnetic platen sensors operate by measuring the change in magnetic coupling as the sensor moves relative to the platen. This is similar to planar motor operation, which is discussed in detail in [8]. The sensor uses its drive coil to create an AC magnetic flux in its drive tooth, which couples into the platen teeth. Depending on the relative location of the platen teeth and the sensor, varying amounts of the flux will return through the two sense teeth. The sense coil is wound around the two sense teeth such that its output is proportional to the difference of the flux in the two teeth. This sensing strategy of varying the medium between two coils to change the magnitude of coupled magnetic flux is essentially the same as in a variable transformer.

The drive coil is excited with an AC signal, which in our system is driven at a frequency of $f_d = 100$ kHz. The output of a sense coil is a modulated AC signal whose amplitude is a function of position. The peak amplitudes occur when one of the sense teeth directly lines up with a row of platen teeth and accepts all of the drive flux, as shown in the left sensor in Fig. 2. The zero amplitude case occurs when each sense tooth overlaps halfway with a row of platen teeth and therefore accepts an equal amount of flux. This case is shown in the right sensor in Fig. 2. In the absence of fringing, the amplitude would vary linearly between these cases since the flux would be strictly proportional to the tooth overlap. This would result in the modulation magnitude being a triangle wave as a function of position. However, fringing increases coupling even in the zero-overlap cases, which decreases the peak output values, causing the modulation function to more closely resemble a sine wave. The sensor output can therefore be approximated by

$$V_s(x,t) = \sin(2\pi x/\tau) \times \sin(2\pi f_d t) \qquad (1)$$

where τ is the pitch of the platen and x is the position of the sensor.

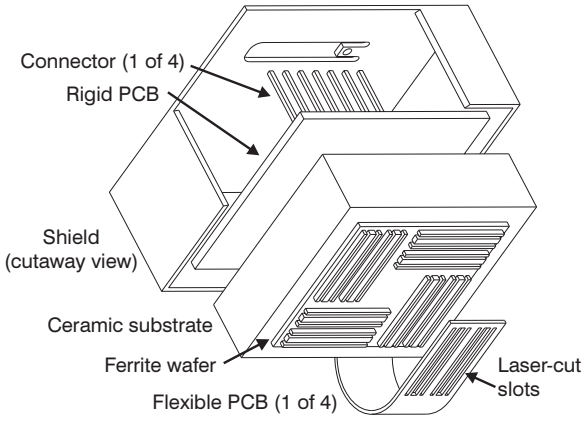

Figure 3: Exploded view of the sensor assembly.

Since this is not a one-to-one function of position, a second sensor channel mounted in "quadrature" is required to recover position. If the second channel is placed $n \pm 0.25$ platen teeth (where n is an integer) away from the first, the modulation of the second channel will be 90° out of phase from the first channel. These two sensors will then form a "quadrature pair" — their outputs are approximately a sine and cosine with respect to position, and so the position of the pair with respect to the platen can in principle be determined. The two sensors in Fig. 2 are separated by 1.25 teeth and are therefore a quadrature pair. This construction is similar to that of a 2-phase planar motor.

Also note in Fig. 2 that the sensor poles (the material surrounded by each coil) are a single tooth wide. In contrast, motors and other sensors use larger poles consisting of multiple teeth. The size of the poles does not affect the fundamental operation of the sensor, but there is a tradeoff to be made between compactness, flux carrying capability and mechanical averaging.

3 Physical Design

Previous sensors of this type have used large steel or ferrite cores wrapped by hand with many turns of wire to produce the drive/sense coil pairs [5, 6]. Our new design stresses reduction of the overall size of the sensor to more easily integrate it with the motor and minimize the amount of mass the motor must carry. It was also important to reduce or eliminate the effects of non-uniformity in the coil winding process. To achieve these goals, we designed a sensor as shown in Fig. 3.

The sensor is based around a single magnetic ceramic (ferrite) substrate which forms all of the sensor teeth. Four flexible printed circuit boards, one for each sensor pair, provide the coils. These aspects of the design are both unlike all previous sensors and are discussed in more detail below. The thin ferrite wafer is bonded to a larger piece of non-magnetic ceramic for stability. The coils are placed over the sensor teeth and bent around the substrate to attach to a connector. The connector is soldered to a small rigid circuit board which in turn is bonded to the back of the substrate. The connector pins fit into sockets on the electronics subassembly (not shown in the figure), giving

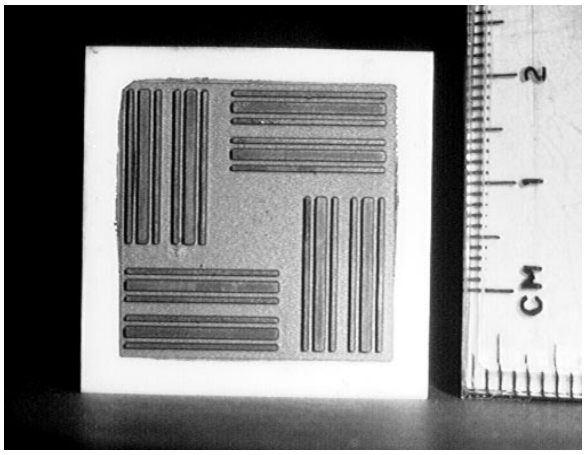

Figure 4: Ultrasonically machined sensor substrate.

the coils both mechanical connection to the back of the substrate and a modular electrical connection to the electronics. The shield encasing the sensor is made of μ-metal, a very high permeability alloy, and isolates the sensor from stray magnetic fields caused by the motor. The sensor assembly (not including the height of the connectors) is approximately $1.3 \times 1.3 \times 0.65$" ($33 \times 33 \times 17$ mm) as built, compared to previous sensors which were as large or larger for a single axis.

The novel substrate works together with the coils to create a sensor that is very compact, yet still provides sufficient signal levels to meet the resolution requirements. The coils, rather than being hand-wound as in previous sensors, are fabricated as traces on flexible printed circuit boards. Each coil is a single "turn", with the drive coil traces on one side of the board and the sense coils on the other. Slots for the sensor teeth are created by laser cutting of the circuit board. This provides for excellent repeatability and consistency between coils — since the length and area of the coils are tightly controlled — which results in predictable resistance and inductance for all coils.

The major disadvantage of a single-turn coil is the low signal strength. Since sensed flux is proportional to the cross-sectional area of the sense coil and therefore to the number of turns, this could be a large problem. However, the MnZn-ferrite material used for the teeth has an initial permeability of $\mu_i \approx 6000$, which greatly increases the flux in the sensor for a given drive current relative to a steel core. The signal levels are not increased to the level of previous sensors, but they are sufficient to provide the required resolution when coupled with the electronics described below.

The ferrite wafer was ultrasonically machined to produce the pattern shown in Fig. 4. This process provides high repeatability of processing and very accurate results, with tolerances on the order of $\pm .02$ mm. It also inherently aligns the four sensor pairs with respect to each other, since they are created simultaneously with a single tool. Additionally, since all aspects of the sensor are essentially planar, it is amenable to batch fabrication.

To integrate the sensor assembly with an existing Northern Magnetics planar motor, a hole was milled out of the center of the forcer. The layout of this particular forcer allowed for the sensor to be permanently integrated with the forcer without changing its footprint. The depth of the hole was tightly controlled so that the sensor teeth would be nearly flush with the bottom of the forcer when the sensor body rested against the bottom of the hole. The sensor assembly was placed in the hole and fixed with potting epoxy. Once the epoxy had cured, the sensor was lapped flush to recreate an air bearing surface. The forcer with integrated sensor can be seen in Fig. 1.

4 Electronic Design/Modeling

An important question with a single turn coil is whether it would be better modeled as a voltage source or a current source. Since it is in effect a variable transformer, either model is reasonable, but the choice affects the way the two halves of the sense coil should be wound. If they are assumed to be current sources, they should be wired in parallel opposition so that the currents subtract directly. If they were wound in series opposition, they would effectively average, reducing the output current by a factor of 2. A similar argument holds for wiring coils modeled as voltage sources in series opposition.

The first version of the electronics was based on a current source model for the sensor, since the voltage developed over a single turn would be very small and measuring it could be problematic. The flexible circuit boards therefore had parallel opposition sense coils and the electronics included a transimpedance amplifier as a first stage. However, initial experimentation indicated that the sensor was behaving as a very poor (low impedance) current source. This caused the amplifier to act as a very high-gain voltage amplifier, severely limiting the available bandwidth. A second version of the electronics therefore uses a voltage source model for the sensor and fast amplifiers in a voltage gain configuration with moderate gain (~ 2500) as a first stage. This works well, although extremely low-noise amplifiers (~ 1 nV/$\sqrt{\text{Hz}}$ input noise) are required due to the small voltage level (< 1 mV) and frequency (100 kHz) of the coil outputs.

After the signal is amplified to a usable level, the magnitude of the sensed AC signal (corresponding to the amount of magnetic coupling in the sensor) must be extracted. The electronics used to do this are outlined in schematic form in Fig. 5. The amplifier output is given by $V_{amp} = A_s(x)\sin(\omega t)$, where $A_s(x) \approx G\sin(2\pi x/\tau)$ is the position-dependent modulation magnitude. This signal is multiplied by the drive signal to get a DC value proportional to the AC magnitude of the sensor output. However, this also produces a signal of equal magnitude at twice the drive frequency:

$$V_m = V_{amp} \times V_d = \frac{A_d A_s}{2}\left[1 + \sin(2\omega t)\right] \qquad (2)$$

where $V_d = A_d \sin(\omega t)$ is the drive signal, and $\omega = 2\pi f_d$ is its frequency in rad/s.

To eliminate this AC signal, a gated integration scheme is used, in which digital circuitry controls

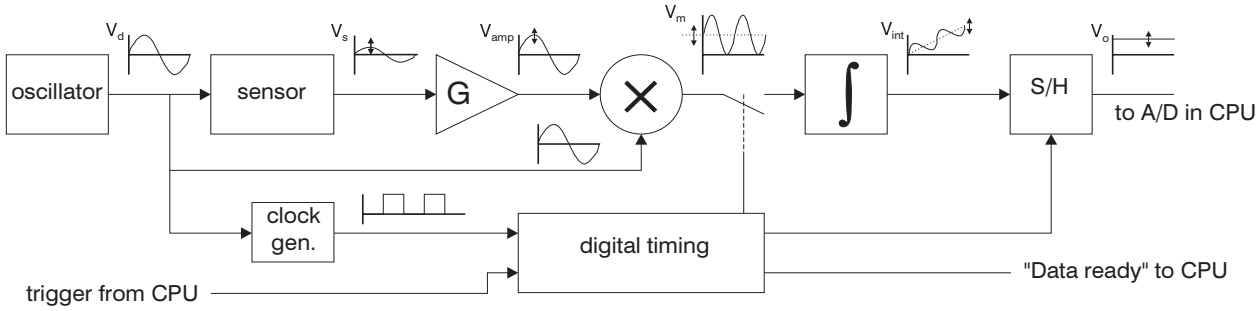

Figure 5: Schematic of the sensor electronics. Representative waveforms are shown along the signal chain.

switches such that the signal of interest is integrated for a finite period of time. In contrast to traditional uses of this circuit, which average many short integrations to recover the amplitude of a noisy AC signal, we are using it as an analog version of a digital boxcar integrator to recover the DC component of a signal in the presence of an AC component at a known frequency. In our case, a digital clock is generated from the drive signal, and the multiplier output signal is integrated for exactly four periods of the drive signal. Since the integral of a sinusoid over an integer number of periods is zero, the output of the integration is simply a constant times the DC value:

$$V_{int} = G_i \int_0^{\frac{4}{f_d}} \frac{A_d A_s}{2} \left[1 + \sin\left(2\omega t\right)\right] dt = \frac{2 G_i A_d A_s}{f_d}$$

where G_i is the gain of the integrator. Since A_d, G_i and f_d are all constant, the output is merely a constant multiple of A_s, the magnitude of the coupling of the sensor. Furthermore, G_i can be varied over a fairly large range to adjust the overall gain of the system. It is also important to note that the preceding analysis is independent of the exact form of A_s.

In practice, the integration is begun with the opening of an analog switch and completed with the transition of a sample and hold amplifier to hold mode. This allows the result of the integration to be read by the computer, which takes a finite period of time.

Also note that in (2), V_{amp} and V_d are assumed to be in phase. In general this is not necessarily true, and phase offset can result in signal loss. However, experiments have shown that the phase difference, which is caused by the inductance of the sensor coils, varies only a few degrees with respect to position. Therefore the drive signal can be phase shifted before multiplication such that the drive and sense signals are always close to phase alignment.

In order to support variable sampling rates, the digital timing circuitry that controls the gated integration can be triggered by an external source, as shown in Fig. 5. The controller triggers the timing circuitry at the desired frequency, and when each integration cycle is complete, the timing circuitry in turn sends a signal that triggers the A/D conversion and sends an interrupt signal to the controller. Since the digital timing cycle takes seven clock cycles to complete, the maximum trigger rate is (100 kHz)/7 = 14 kHz.

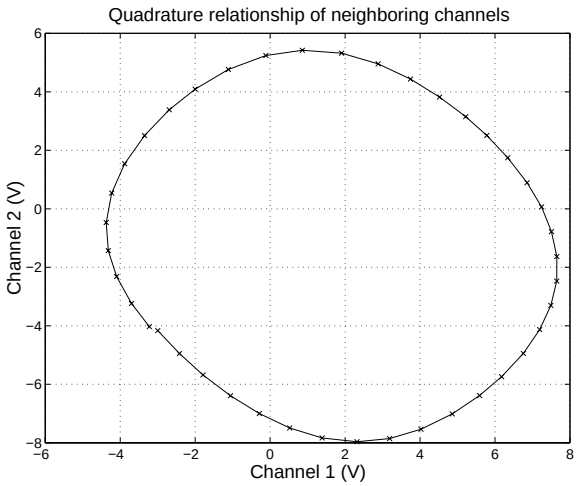

Figure 6: Quadrature relationship between neighboring channels.

The electronics have all been implemented on a single circuit board which sits inside the forcer housing and connects directly to the sensor. Only the power, DC outputs and digital control signals travel along a cable attached to the motor's tether.

5 Results

5.1 Functional verification

Preliminary experiments were performed to verify the basic operation of the sensor. For these tests, the integrated forcer/sensor was microstepped across the platen and the sensor outputs were recorded at each position. In this section, "sensor outputs" will refer to the DC outputs of the electronics as recorded by the A/D converter in the controlling computer. Fig. 6 presents results from one such experiment, showing the quadrature relationship of a sensor pair. The motor performed 25 μm steps, and the mean of 50 samples was recorded for each sensor at each step. The basic form of the sensor outputs as a function of position can also be verified from this plot. Triangle waves from each sensor would produce a diamond-shaped quadrature figure, whereas a sine and cosine would give a perfect circle. The quadrature figure in Fig. 6 is between these cases, and closer to a circle, as expected.

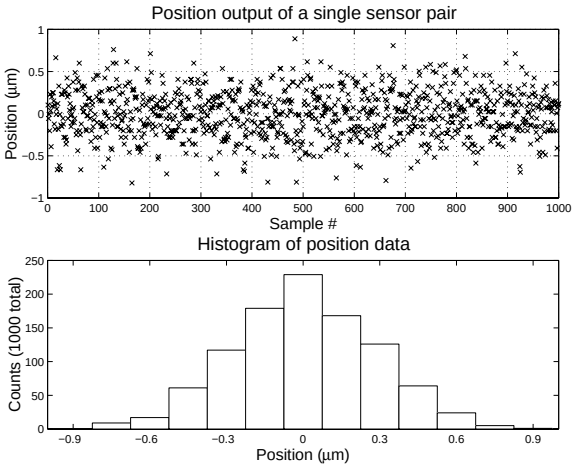

Figure 7: Calculated position from a single sensor pair, σ=0.27 μm, shown as a function of time (recorded at 3 kHz) and as a histogram.

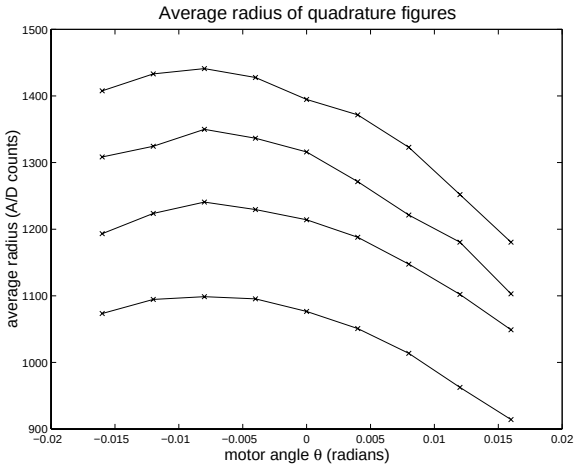

Figure 8: Average radius of quadrature circles as a function of motor angle.

To calculate position for each quadrature pair, we assume that the sensor modulation is sinusoidally dependent on position. This assumption introduces some inaccuracies, which are discussed in Section 5.4, but in general the inaccuracy is less than 10% over small displacements, so it is valid to estimate sensor resolution from uncalibrated position measurements. Position is calculated by taking the arctangent of the two values relative to the center of their quadrature figure, and multiplying by $\tau/2\pi$, where τ =1.016 mm is the pitch of the platen, to convert from radians to mm.

5.2 Sensor resolution

For the purposes of this section, resolution is defined as the standard deviation (σ) of the noise of the sensor position. To determine resolution experimentally, sensor data was collected at 3 kHz with the motor amplifiers on and the forcer stationary. A laser interferometer was used to verify that the forcer was not moving significantly during this experiment. This turned out to be a major concern, since in general the motor may vibrate from 0.1 μm to 1.0 μm peak-to-peak under open-loop control. Position was calculated from each sensor pair using the arctangent method described above. Data from one sensor pair during this experiment is shown in Fig. 7. Analysis of these data shows that the resolution of the four pairs was between $\sigma = 0.26\,\mu$m and $\sigma = 0.32\,\mu$m.

To determine the position of the center of the forcer, the outputs of the two sensor pairs in each direction are transformed from their relative values to absolute values and averaged together. Since the noise is not systematic, this improves resolution. For the experiment described above, this resulted in resolutions of $\sigma = 0.20\,\mu$m and $\sigma = 0.21\,\mu$m for the two axes. A number of experiments proved these values to be typical for the system. Experiments were also performed in which the forcer stepped across the platen in 40 μm increments while data was taken at each position. These verified that the sensor noise is independent of position.

During the stepping experiments, off-axis sensitivity was also investigated. Due to fabrication variations, the length of the sensor teeth will not be exactly an integer times the platen pitch, as desired. This will cause the magnetic coupling in the X sensors to be a weak function of position in Y, and vice versa, causing apparent motion in the direction orthogonal to actual motion. The apparent orthogonal motion during these experiments was no greater than $\pm 1\,\mu$m and so can generally be ignored. Experiments were also performed with the amplifiers off and the motor stationary at various points on the platen, to determine the effect of the nearby motor currents on the sensor. Under these conditions, the sensor signals had noise equivalent to 0.23–0.26 μm, or about 15% less than with the amplifiers on. Examination of systematic effects of motor currents on sensor position outputs is underway.

5.3 Rotational effects

Forcer rotation has two different effects on the sensor. First, as the forcer rotates, the sensor teeth will no longer align exactly with the rows of platen teeth, and the sensor signals will decrease. This can be measured by examining the change in size of the quadrature figures as the motor is rotated. The average radius of the four quadrature figures (one for each sensor pair) as a function of motor angle θ is shown in Fig. 8. These curves appear to match the analytical functions developed by Ish-Shalom [9]. This also indicates that the as-built sensor teeth are not exactly parallel to the motor teeth since the maximum signal is not at θ=0, but that the sensor was mounted about 8 mrad (0.4°) from square. The second effect of motor rotation is that the two sensor pairs in each axis will appear to move relative to each other as the motor rotates. This is because the sensors measure distance along each axis of the platen, and therefore the apparent distance between the two pairs in each direction is the projection of their separation onto that axis.

Because the radii of the quadrature figures are not constant with respect to position (i.e. they are not

perfect circles), it is not obvious how to use the signal dropoff to directly measure position, but rather some calibration would be required. Instead, we simply calculate angle by calculating the apparent distance between sensors in each direction and dividing the change in this distance from nominal by the lever arm. Although this does not use all the available information to determine rotation, it does allow all four sensor pairs to be used to determine angle, minimizing noise effects. This calculation gives motor angle with a noise level of $\sigma = 25\mu$rad (.0014°).

5.4 Calibration/Accuracy

In practice, the modulation of the sensor outputs is not an exact sinusoid, which causes the quadrature figure to be non-circular, as can be seen in Fig. 6. Also, the angle around the figure is not linear with respect to position. These cause the arctangent calculation to give a somewhat inaccurate result, as can be seen in Fig. 9. The inaccuracy of the uncalibrated sensor in this plot is about $\pm 16\,\mu m$. The inaccuracy of other sensor pairs was seen to be as large as $\pm 25\,\mu$m. These data were obtained by calculating sensor positions using the arctangent method and comparing those positions to those reported by the laser interferometer.

Comparing experimental data from various points on our platen reveals that approximately half of this inaccuracy is due to the assumption of sinusoidal sensor outputs, while the remaining inaccuracy is primarily due to variations in the platen tooth geometry. While the former can in principle be entirely calibrated out, the latter is a function of the tolerance of the platen teeth and is unavoidable. To perform sensor calibration, a 16th order polynomial was fit to the inaccuracy curve for each of the four sensor pairs. These polynomials are then used to generate more accurate sensor positions. Over a single platen tooth, calibration worked extremely well, as was expected, reducing inaccuracies to less than 1 μm. However, for use with a controller over the entire platen, the inaccuracy curves used to calibrate against were generated from a large data set composed of many trials at different points on the platen. This essentially calibrates the sensor to an "average" platen tooth, with the variations in tooth shape responsible for the remaining inaccuracy. The results of this calibration can be seen in Fig. 9. This particular data set has residual inaccuracy of about $\pm 6\,\mu$m, although other data sets have shown inaccuracies as large as $\pm 9\,\mu$m.

6 Conclusion

We have presented both the physical and electronic design for a new magnetic sensor for planar linear motors. This sensor is significantly smaller than previous sensors and senses three degrees of freedom with sufficient resolution to support high-performance closed-loop control. Experimental results were presented that demonstrate position resolution of $\sigma = 0.2\,\mu$m in both X and Y and angular resolution of $\sigma = 25\,\mu$rad in θ at a sampling rate of up to 14 kHz. Results of calibration experiments were also presented which give the sensor a global accuracy of better than 10 μm. The sensor has been used to successfully run the motor under closed-loop control, as described in [10].

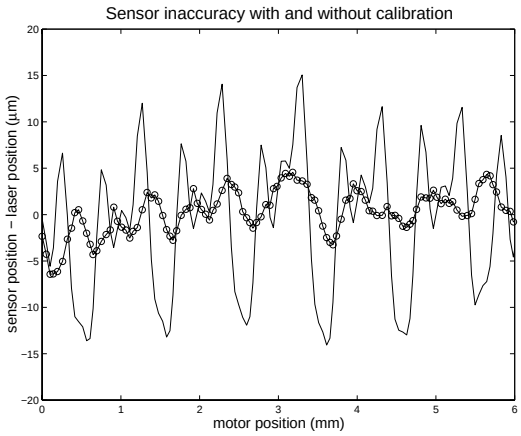

Figure 9: Inaccuracy of one uncalibrated (plain line) and calibrated (line with circles) sensor pair.

Acknowledgments

This work was supported in part by NSF grants DMI-9523156 and DMI-9527190. Zack Butler was supported in part by an NSF Graduate Research Fellowship. Alfred Rizzi was supported in part by NSF grant CDA-9503992. The authors would like to acknowledge Arthur Quaid for his input and assistance with the experimental setup.

References

[1] L. M. Clark, "Linear Motor Technology for SMD Placement" in *Proc. 5th Int'l SAMPE Electronics Conf.*, Boston, June, 1991.

[2] A. A. Rizzi, J. Gowdy, and R. L. Hollis, "Agile Assembly Architecture: An Agent-Based Approach to Modular Precision Assembly Systems" in *Proc. Int'l Conf. on Robotics and Automation*, pp. 1511-1516, April, 1997.

[3] B. D. Hoffman and S. H. Pollack, U.S. Patent 4,823,062.

[4] G. L. Miller U.S. Patent 4,958,115.

[5] D. Crawford, F. Y. Wong, and K. Youcef-Toumi, "Modeling and Design of a Sensor for Two Dimensional Linear Motors" in *Proc. Int'l Conf. on Robotics and Automation*, pp. 2367-2372, May, 1995.

[6] J. Ish-Shalom, "Sawyer Sensor for Planar Motion Systems" in *Proc. Int'l Conf. on Robotics and Automation*, pp. 2652-2658, May, 1994.

[7] A. E. Brennemann and R. L. Hollis, "Magnetic and Optical-Fluorescence Position Sensing for Planar Linear Motors" in *Proc. Int'l Conf. on Intelligent Robots and Systems*, vol. 3, pp. 101-107, August, 1995.

[8] W. E. Hinds and B. Nocito, "The Sawyer Linear Motor" in *Theory and Application of Step Motors* (B. Kuo, ed), pp. 327-340, St. Paul, West Publishing Co., 1974,

[9] J. Ish-Shalom, "Modeling of Sawyer Planar Sensor and Motor Dependence on Planar Yaw Angle Rotation" in *Proc. Int'l Conf. on Robotics and Automation*, pp. 3499-3504, April, 1997.

[10] A. E. Quaid and R. L. Hollis, "3-DOF Closed-loop Control for Planar Linear Motors" Submitted to 1998 Int'l Conf. on Robotics and Automation.